CO_2 Enhanced Chemical Vapor Deposition Growth of Few-Layer Graphene over NiO_x

In Hyuk Son,[†,#,*] Hyun Jae Song,[†,#] Soonchul Kwon,[†] Alicja Bachmatiuk,[‡,§,⊥] Seung Jae Lee,[†,▽] Anass Benayad,[†] Jong Hwan Park,[†] Jae-Young Choi,[†] Hyuk Chang,[†] and Mark H. Rümmeli[‡,∥,*]

[†]Samsung Advanced Institute of Technology, Samsung Electronics Company, LTD, 130 Samsung-ro, Yeongtong-gu, Suwon-si, Gyeonggi-do 443-803, Republic of Korea, [‡]IBS Center for Integrated Nanostructure Physics, Sungkyunkwan University, Suwon 440-746, Republic of Korea, [§]Centre of Polymer and Carbon Materials, Polish Academy of Sciences, M. Curie-Sklodowskiej 34, Zabrze 41-819, Poland, [⊥]IFW Dresden, Institute of Complex Materials, P.O. Box 270116, D-01171 Dresden, Germany, and [∥]Department of Energy Science, Department of Physics, Sungkyunkwan University, Suwon 440-746, Republic of Korea. [#]These authors contributed equally to this work. [▽]Present address: Marine Research Institute, Samsung Heavy Industries Co. Ltd., Gyeongsangnam-do 656-710, Republic of Korea.

ABSTRACT The use of mild oxidants in chemical vapor deposition (CVD) reactions has proven enormously useful. This was also true for the CVD growth of carbon nanotubes. As yet though, the use of mild oxidants in the CVD of graphene has remained unexplored. Here we explore the use of CO_2 as a mild oxidant during the growth of graphene over Ni with CH_4 as the feedstock. Both our experimental and theoretical findings provide in-depth insight into the growth mechanisms and point to the mild oxidants playing multiple roles. Mild oxidants lead to the formation of a suboxide in the Ni, which suppresses the bulk diffusion of C species suggesting a surface growth mechanism. Moreover, the formation of a suboxide leads to enhanced catalytic activity at the substrate surface, which allows reduced synthesis temperatures, even as low as 700 °C. Even at these low temperatures, the quality of the graphene is exceedingly high as indicated by a negligible D mode in the Raman spectra. These findings suggest the use of mild oxidants in the CVD fabrication as a whole could have a positive impact.

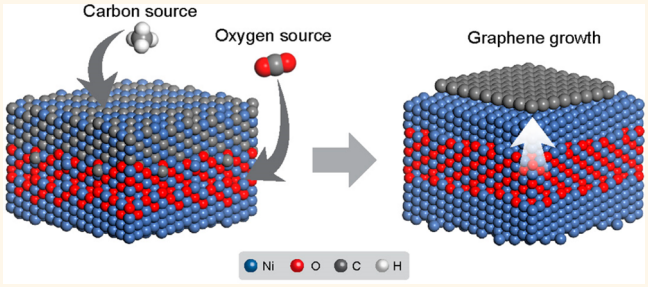

KEYWORDS: chemical vapor deposition · CVD · Ni · CO_2 · graphene

In the early days of graphene synthesis by chemical vapor deposition (CVD), there was great hope for the use of Ni as a catalyst given its immense success as a catalyst for carbon nanotube (CNT) fabrication. However, Ni has a high carbon solubility at elevated temperatures[1,2] as well as high carbon diffusivity[3] making the controlled CVD growth of graphene over Ni somewhat challenging. This led to the emergence of Cu as a catalyst which allows a greater degree of growth control due to its significantly lower carbon solubility at elevated temperatures. That along with the challenges of implementing Ni as a catalyst meant most researchers turned to Cu as a catalyst for graphene growth.[4,5] Nonetheless, some studies using Ni as a catalyst continue and some of the challenges are beginning to be overcome. For example, the use of Ni–Mo alloys can lead to the formation of large area homogeneous monolayer graphene,[6,7] or in the case of Ni–Au alloys, low temperature growth of graphene at 450 °C is possible.[8]

In terms of the growth mechanisms underlying CVD graphene formation using Ni catalysts, while numerous growth modes have been proposed, two primary mechanisms seem to have been identified. In the first, carbon species are formed by the catalytic decomposition of the hydrocarbon feedstock which then dissolve C species in to the bulk Ni substrate forming a stable Ni–C solution which upon initial cooling leads to a condensed graphene layer forming on the surface and is known as the segregation step. With further cooling phase-second proposed mechanism, graphene formation can occur entirely at the Ni catalyst surface probably at step edges, *i.e.*, segregation does not occur. This second mechanism is argued to occur at low temperatures[8,10] and has also been identified to occur when using alcohol as the hydrocarbon feedstock.[9]

* Address correspondence to inhyuk74.son@samsung.com, mark@rummeli.com.

Received for review June 2, 2014 and accepted August 29, 2014.

Published online August 29, 2014
10.1021/nn504342e

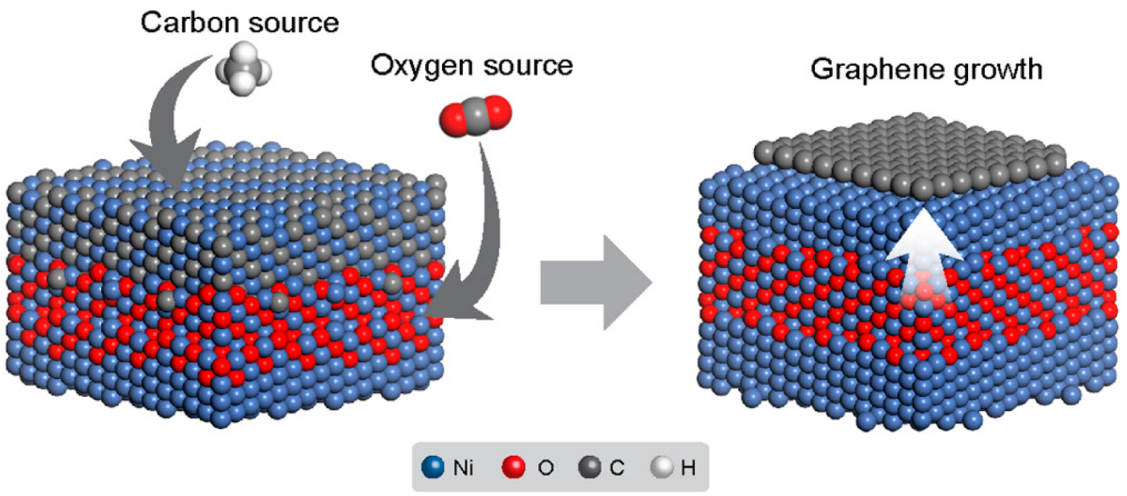

Figure 1. Schematic diagram of graphene growth over a NiO_x surface. CO_2 serves as the mild oxidant in the reaction and provides the means to form NiO_x at the surface.

Both these graphitization mechanisms are in agreement with the formation mechanisms identified in segregation studies in which Ni had been preloaded with C atoms by ion implantation.[2,11] Those studies identified graphene formation by surface precipitation and through surface nucleation at step edges. Thus, it seems depending on the synthesis conditions one of these two graphene formation processes dominates when using Ni as the substrate/catalyst.

Aside from the usual synthesis parameters (*e.g.*, temperature, cooling rate, feedstock type, hydrogen concentration etc.), another option that can alter growth is by the introduction of a gaseous oxidizer. The use of weak oxidizers in enhancing carbon nanotube growth was enormously successful. Early work employed water vapor to form remarkably long CNTs, the so-called "super growth" of CNTs.[12] This lead to numerous studies with oxygen containing gases in the CVD growth of CNTs. The studies showed that oxygen containing gases have the ability to modulate the CNT structures[13−15] as well as prolong the life of the catalyst particles and prevent their sintering.[12,16,17] In addition, it is argued that weak oxidizers prevent amorphous carbon build up that can poison the catalyst particles and interfere with sp^2 carbon growth. Of the weak oxidizing gases explored, CO_2 showed great promise and is superior to water vapor in that its flow rate is more easily controlled and it does not condense in pipelines at room temperature.[18] Despite the success of weak oxidizers to enhance CVD grown CNT, thus far few, if any, such studies have been explored for the CVD synthesis of graphene.

In this study we focus on the use of Ni as a catalyst/substrate and the use of weak oxidizers during the CVD growthwater process (Figure 1). Most of the study investigates the use of CO_2 rather than H_2O, although preliminary studies with H_2O are also presented. We choose CO_2 not only for its superior control in the reaction as compared to H_2O, but also for the utilization of CO_2 regarded as the major contributor of a greenhouse gas. Thus, if such a CVD process using CO_2 gas where to be scaled up this could be considered environmentally friendly assuming CO_2 from the atmosphere were used.

RESULTS AND DISCUSSION

To unambiguously determine if graphene is present, we use Raman spectroscopy after transferring the material to Si/SiO_2 substrates. Three primary peaks at *ca.* 1350 cm^{-1} (D mode), *ca.* 1600 cm^{-1} (G mode) and *ca.* 2700 cm^{-1} (2D mode) can be used to determine the presence of graphene. We detect these signatures for samples fabricated with or without the presence of CO_2 in the reaction as can be seen in Figure 2 which shows a typical Raman spectrum for graphene fabricated with or without CO_2 during the CVD reaction. A rather obvious feature when comparing these two spectra is that of the relative intensity of the D mode between the spectra. In the case of the CVD reaction with no CO_2, the D mode is relatively high as compared to the G mode ($I_D/I_G \sim 0.42$). The D mode is a forbidden transition that becomes allowed due to defects (broken symmetry) and thus the I_D/I_G can be used as a means to evaluate the quality of graphene. The high I_D/I_G for samples produced without CO_2 indicates a very defective material. This is not unexpected since in this case the graphene synthesis occurred at the relatively low temperature of 700 °C. Typically, graphene synthesis over Ni using methane as the feedstock occurs at 900−1100 °C. However, when CO_2 is used in the reaction, the D mode can hardly be discerned ($I_D/I_G \sim 0.02$) indicating that the presence of CO_2 leads to high quality graphene. The I_{2D}/I_G and the fwhm of the 2D can be used to evaluate the number of layers.[19] In the case of the no CO_2 being used in the reaction the I_{2D}/I_G and the fwhm of the 2D values are 0.56 and 100 cm^{-1}, respectively, suggesting few layer graphene of more than 10 layers. With CO_2 introduced

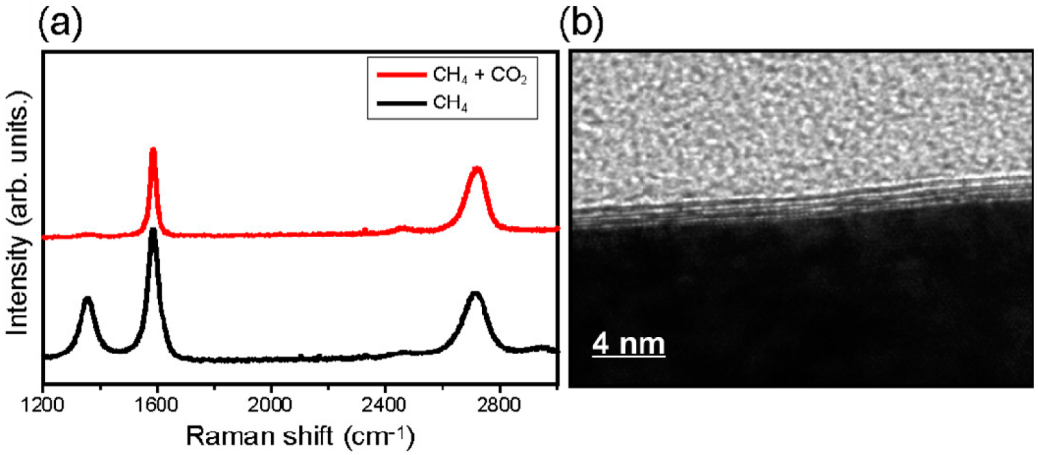

Figure 2. (a) Raman spectra for graphene growth using CO_2 with CH_4 (red) and CH_4 without CO_2. The large D mode at *ca.* 1350 cm^{-1} without CO_2 is easy to see. This indicates the quality of the graphene produced with CO_2 in the reaction is significantly better. (b) TEM image of a cross section showing few layer graphene (grown with CO_2 and CH_4) over the Ni substrate.

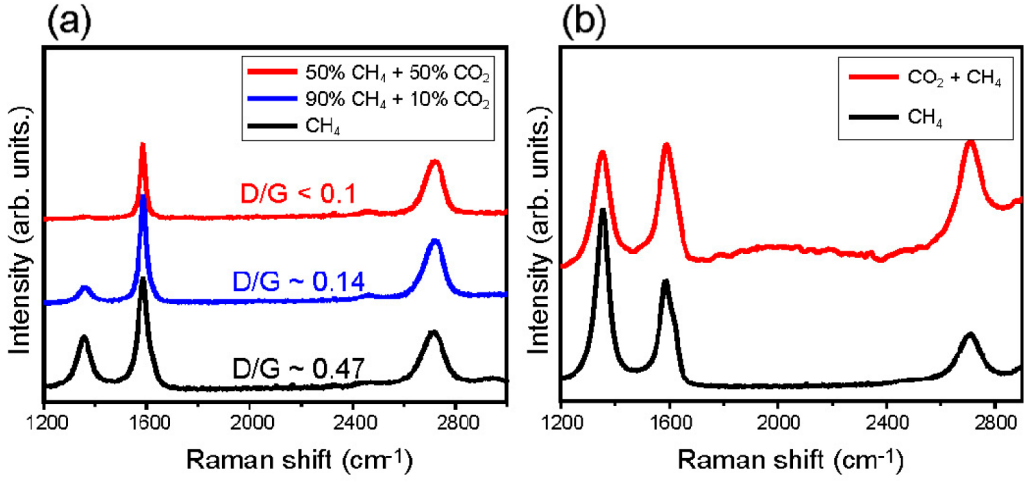

Figure 3. (a) Raman spectra showing the effect of CO_2 concentration on graphene growth growth. (b) Comparison of low temperature growth (500 °C) with and without CO_2 in the reaction. With CO_2, the D mode is reduced indicating improved graphene formation.

into the reaction the I_{2D}/I_G drops to *ca.* 0.68 and the fwhm of the 2D is *ca.* 80 cm^{-1} suggesting few layer graphene between 3 and 5 layers. Moreover, the width of the 2D mode suggests AB stacked few layer graphene.[19] We also looked at the reaction time dependency with respect to layer number for 10, 20, and 30 min reactions (with CO_2). No dependence was observed as shown in figure S2 in the Supporting Information. We also explored the role of CO_2 ratio with respect to the CH_4 feedstock. Figure 3a shows the improvement in I_D/I_G for two CO_2 concentrations (10% and 50% CO_2). The improvement in I_D/I_G as compared to no additional CO_2 is obvious, and moreover, with 50% CO_2, the D mode is well below 0.1, *i.e.*, it is negligible. In addition as the CO_2 ratio increased the I_G/I_{2D} reduces indicating a reduction in the number of graphene layers. For CO_2 fractions greater than 50% no further improvement in graphene quality is observed and the graphene coverage over the substrate is found to deteriorate. The potential of CO_2 to improve the quality of the as-produced graphene at lower temperatures was also investigated. Figure 3b shows the Raman spectra for graphene grown with a reaction temperature of 500 °C with and without the addition of CO_2. Again the improved quality (reduced D mode) when adding CO_2 is clear.

An interesting question is whether any carbon from the CO_2 is used in the graphene formation. To check this we explored the use of ^{12}C (99%) and ^{13}C (99%) enriched CO_2 gas in the reaction. Since the molecular vibrational frequencies are inversely proportional to the mass ($\omega^2 \propto 1/m$) where ω is the frequency and m is mass any change in C isotope ratio will lead to an overall shift of peaks in the Raman spectra.[20,21] Figure 4 shows the Raman spectra for graphene obtained with ^{12}C and ^{13}C enriched CO_2 compared to graphene

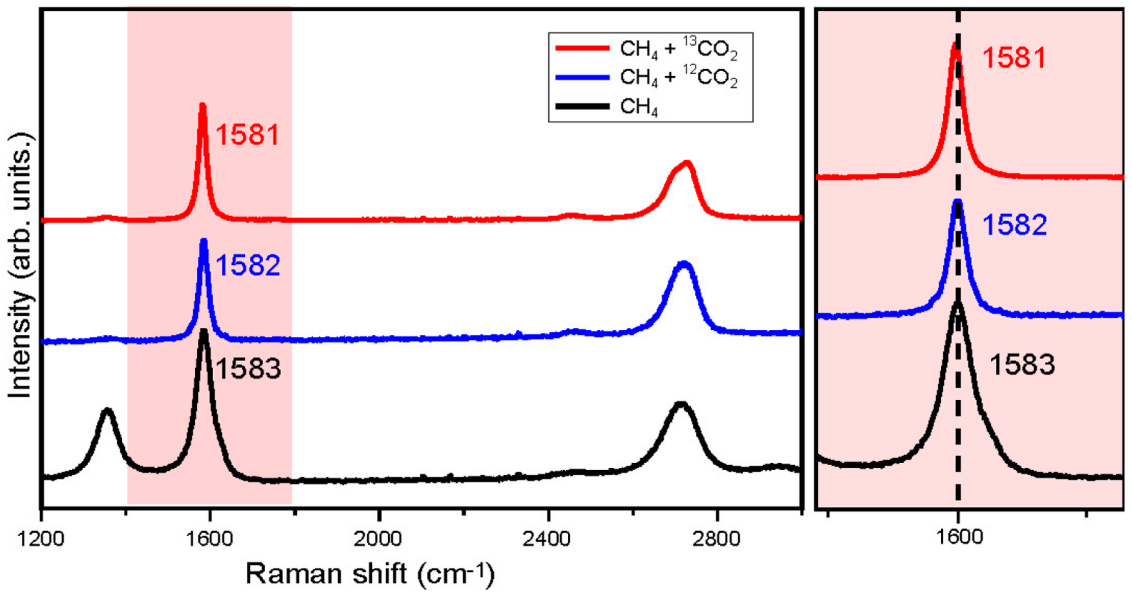

Figure 4. Raman spectrum of graphene with isotope labeled CO_2 assisted growth. No shift in the G and 2D modes is observed indicating the carbon feedstock for graphene growth comes from decomposed CH_4 and not CO_2.

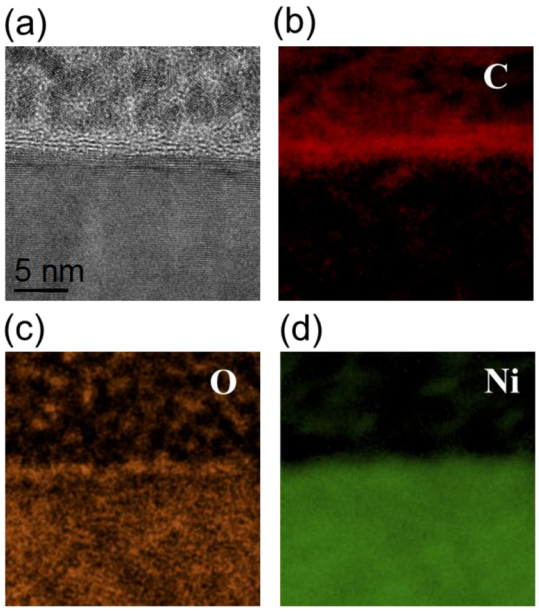

Figure 5. (a) Cross-sectional TEM image of few layer graphene over NiO_X. Corresponding Energy Filtered TEM in false color for (b) C, (c) O, and (d) Ni. No carbide formation is observed.

fabricated with no CO_2. Within the error no shift is observed indicating that carbon from the CO_2 is not used in the growth of the graphene, *viz.* carbon derived from decomposed CH_4 is used to grow the graphene.

The use of a mild oxidizer (CO_2) in the reaction clearly improves the quality of the produced graphene and reduces the number of graphene layers forming on the Ni substrate. To better comprehend the role of the mild oxidizer on Ni, we conducted HRTEM investigations on cross-sectional samples and X-ray photoemission spectroscopy (XPS) at sequential depths. Figure 5a shows the cross-sectional HRTEM image of such a focused ion beam (FIB) lamella prepared. At the top one sees the Pt particles deposited to protect the surface during the FIB lamella production process. Below the protection layer a few layers of graphene are visible and under that lies the Ni substrate. In Figure 5, panels b–d show energy filtered TEM images for C, O and Ni, respectively, with each indicated in false color. The C energy filtered image shows no significant C presence in the Ni. However, the oxygen map shows some oxygen in the Ni, at least near the surface in the measured region. While O could arise from exposure to air it is unlikely as the data was HRTEM data was collected immediately after sample preparation. However, to better study this point systematic depth studies using XPS were conducted. During this process the sample is measured and then a little of the surface is removed by a special sputtering process and then the sample is remeasured and so forth. During these measurements the sample is never exposed to air or an oxidant. In Figure 6, panels a–c show the core level peaks for C, Ni and O, respectively, with respect to sputtering time (depth). For the C 1s peak at the surface (top profile), the C 1s peak corresponds to sp^2 carbon with a peak centered at 284.3 eV.[22,23] Then the relative C 1s intensity drops as one gets even deeper (between 6 and 8 nm).

For the C 1s edge at the surface (top profile), the C 1s peak corresponds to sp^2 carbon with a peak centered at 284.3 eV.[23] Then the relative C 1s intensity drops. As one gets even deeper (between 120 and 150 s), the profile starts to show a small shoulder 283.6 and 835.5 eV which can be attributed to Ni_3C[22] suggesting small amounts of C get trapped deeper in the Ni substrate. The Ni $2p_{3/2}$ edge profile shows a peak at *ca.* 852.6 eV

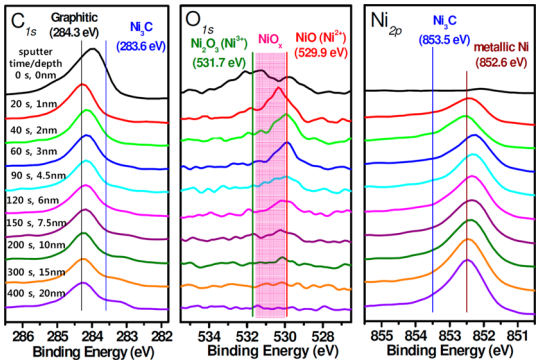

Figure 6. XPS core peak depth profiles of C_{1s}, O_{1s} and $Ni_{2p3/2}$ for a sample of graphene grown over Ni with CO_2 in the reaction. Signatures for oxygen near the surface are easily observed at O_{1s}.

concomitant with Ni throughout except for the first measurement where it is negligible as one would expect as this is where the graphene resides. The O 1s edge initially shows a weak double hump feature between 529.9 and 531.7 eV, assigning NiO_x.[24] The C 1s spectrum profile starts to show a small shoulder at 283 eV which is attributed to Ni_3C[22] suggesting small amounts of C get trapped deeper in the Ni substrate. The Ni_{2p} core peak registered at the surface indicates the presence of a main peak centered at 852.6 eV assigned to Nickel in a metallic environment. The weak oxygen species disappear further in to the bulk suggesting a Ni suboxide exists at the surface of the Ni film concomitant with the TEM data.

DISCUSSION

The experimental data point to the inclusion of weak oxidizers in a (low temperature) CVD reaction massively improving the quality of the graphene. This has been observed previously in the case of synthesized single wall carbon nanotubes (SWNT) by laser ablation.[25] In that case, upon the addition of H_2O to the reaction, the G/D for the SWNT improved enormously, exactly as we find here. The reason for this massively improved crystallinity in the graphene can be attributed in part to a reduction in amorphous carbon species in the system.[12,14−18] In addition, oxygen containing gases have been shown to accelerate graphitization.[26] However, the mechanisms involved are far less understood.

The Catalytic Interaction between CO_2 and CH4 with Ni (111) Surfaces. To better comprehend the role of the reactant gases in our reaction, we conducted density functional theory (DFT) calculations to investigate the structural deformation and binding energetics between CO_2/CH_4 and Ni (111) as shown in Figure 7a,b (see also Table S1 in the Supporting Information). We optimized the geometry of Ni (111) with a CO_2 (panel a) or CH_4 (panel b) molecule at the surface to evaluate the adsorptive configuration. At the available adsorption sites of Ni (111), a relatively strong bond (bond length = 1.86 Å) for the Ni−CO_2 configuration was achieved, while a relatively weak bond (bond length = 2.27 Å) for the Ni−CH_4 configuration was obtained. In addition, the binding energy for the Ni-CO_2 system (−2.21 eV) is higher than that for the Ni−CH_4 system (−2.15 eV), suggesting that CO_2 adsorption is preferable at the Ni (111) surface. These results are consistent with the interpretation of the energy trends in terms of molecular orbitals. Since the degree of electron delocalization allows a change in the HOMO (highest occupied molecular orbital) /LUMO (lowest unoccupied molecular orbital) band gap, different reactant gases show different changes in molecular orbitals with Ni (111) interaction. The small band gap of the Ni−CO_2 system indicates that not much energy is required to excite the molecule, allowing CO_2 to interact with Ni (111) more easily as compared to that of the Ni−CH_4 system. In short, the HOMO−LUMO band gap and binding interaction of CO_2−Ni (111) system suggest that CO_2 can interact with Ni (111) more readily than CH_4 during competitive adsorption of CO_2 and CH_4.

The Importance of NiO_x. Given the fact that the C isotope studies show C from CO_2 do not significantly contribute to the graphene formation, yet experimentally oxygen species are found in the Ni surface (NiO_x), this suggests CO_2 decomposes at the Ni surface to O, which diffuses into the Ni, and releases CO, which might serve as an accelerant gas for graphitization. To better comprehend the role of NiO_x, we first look at the different levels of oxygen that might incorporate into the Ni system. In Supporting Information Figure S4a,b, we show the partial density of states PDOS at the Fermi level for the carbon s-orbital in graphene on NiO with O surface termination and NiO_x with Ni termination below an initial Ni layer. For the case of graphene over O terminated NiO, no PDOS is shown at the Fermi level indicating graphene formation on O terminated NiO is not favorable. Whereas in the case of Ni terminated NiO_x with O residing a few atom layers below a Ni surface, a PDOS is achieved at the Fermi level. This indicates that such a system is favorable for graphene formation. Since the carbon p-orbitals are more dominant at the interface, we also calculated the PDOS for the carbon p-orbital in graphene on O terminated NiO (Supporting Information Figure S4b) and Ni terminated NiO_x (Supporting Information Figure S4d). In the same manner, Ni terminated NiO_x shows a stronger intensity at the Fermi level, which is in the line with the above discussion for the carbon s-orbital. In particular, this remains favorable for bilayer graphene (Supporting Information Figure S4e,f) suggesting layer by layer graphene formation. In addition, we evaluated a simulation of optimized geometry of graphene adsorbed NiO_x (Gr/NiO_x) in which we compared the simulated Ni d orbital for Gr/NiO_x with our experimental data (Figure 7c,d). In particular, the experimental valence

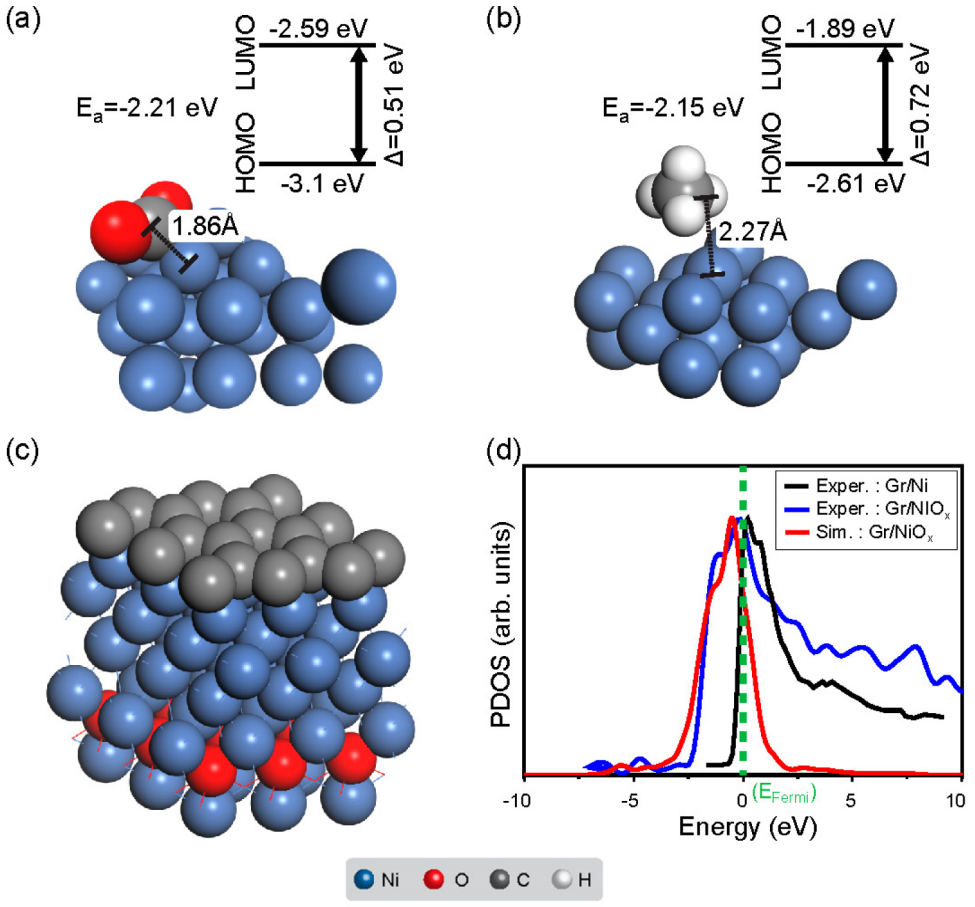

Figure 7. Adsorptive configuration of CO_2/CH_4 and graphene on Ni and NiO_x using DFT calculations (a–c). (d) PDOS comparing theory and experiment. The Fermi levels match for NiO_x.

band structure for graphene on Ni (Gr/Ni) is presented in Figure 7d. The simulated density of states from the Fermi level to the first highest occupied state matches that obtained experimentally for graphene over a NiO_x system confirming that in the presence of weak oxidizers (*e.g.*, CO_2) Ni terminated NiO_x forms.

The experimental DOS from the XPS valence band of Gr/Ni and Gr/NiO_x has a mainly nickel d orbital character as the cross section of metal 3d photoelectrons is higher than that for the sp carbon photoelectron in XPS measurements. However, in Gr/Ni system, we can distinguish two main structures, a nearly triangular shape band near Fermi level assigned to the 3d9s1 configuration, while the 3d84s2 configuration induced the satellite peak around 6 eV. In the case of Gr/NiO_x the O 2p–Ni 3d hybridization gives rise to two main photoemission final states, 3d8L-1 and 3d9L-2 (L is ligand (O 2p) density of state) character with charge transfer from the adjacent oxygen atoms. The adsorbed oxygen at the surface of nickel induced metal–ligand charge transfer screening gives rise to a broad satellite structure at higher binding energies as seen in the valence band of Gr/NiOx system in Figure 7.[27] It is worth noting that the change in d-band electronic structure by oxygen adsorption from CO_2 molecules affects the coupling matrix (pd) which mixes the d orbitals of nickel and the p orbitals of carbon (π and σ) to form either sp^2-like (graphene) or sp^3-like (NiC) carbon. In essence the oxygen atoms tune the catalytic properties of Ni valence orbitals, which directly improve the graphene growth mechanism.

Carbon Diffusion. We also explore the reaction pathways for C diffusion in Ni as compared to NiO_x. In Figure 8a, we show the reaction pathways for CH_4, and its reaction intermediates CH_3, CH_2 and C on Ni and NiO_x for their chemisorption and then decomposition. The simulation is based on that developed by Mueller *et al.*[28] Our adsorption energies for the intermediates on Ni (111) are in excellent agreement with ref 28 for the Ni (111) (see Table S3 in the Supporting Information). Moreover, the study shows that while the stepwise decomposition of CH_4 to C is endothermic (*viz.* elevated temperatures are required for the decomposition), the reaction pathway is more favorable on NiO_x (111) than on Ni (111) at lower energies in the final decomposition steps. We then look at the role of a an NiO_x layer as compared to Ni (see Figure 8b) and find that carbon diffusion in the NiO_x (111) system is more difficult as compared to Ni (111). This suggests that the oxygen layer of NiO_x layers may inhibit C diffusion

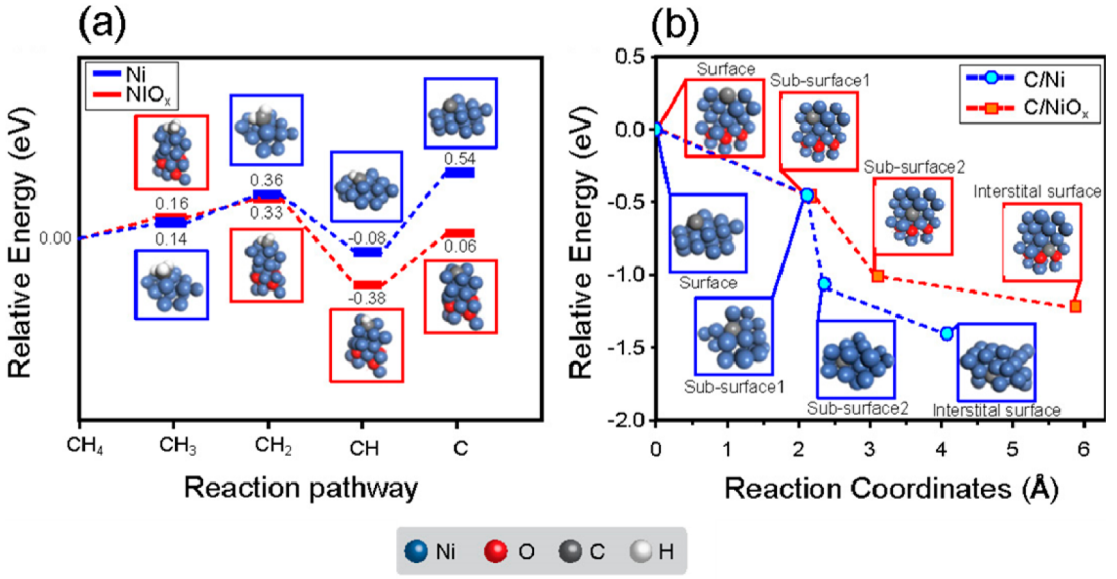

Figure 8. Calculated CH_4 dissociation pathways on Ni (111) and NiO_x (111) (a), and for carbon diffusion on Ni and NiO_x (b).

and this explains the reduced number of graphene layers we find experimentally when using CO_2 as compared to the CVD reaction without CO_2. Moreover, this hints that graphene formation occurs as a surface process rather than by carbon precipitation. This would be in keeping by studies by Maruyama *et al.*[9] in which they grew graphene of Ni using ethanol as the feedstock. Ethanol provides a source of oxygen and one can realistically anticipate they also had NiO_x formation. In addition, they showed their graphene formation was dominated by surface processes as compared to carbon dissolution and precipitation. Both our experimental and theoretical data point to a surface process in which graphene forms on Ni terminated Ni suboxide with layer by layer graphene formation occurring at the surface.

It is also worth looking at how this study compares with a recent study on the role of oxygen species on the surface of Au. In CVD graphene growth over Cu, growth is typically a surface process in which growth is limited by C edge attachment to a growing island. However, Hao *et al.* (ref 29) showed that with the presence of oxygen species at the Cu surface passivate nucleation. Hence, by controlling the O species, they were able to control the nucleation density and in this way they could obtain centimeter-scale graphene domains. In essence, by controlling the surface oxygen species, they could change the growth kinetics from edge-attachment-limited to diffusion-limited. In the same way, we might expect surface oxygen species on Ni to passivate nucleation in agreement with our theoretical observations.

CONCLUSION

In this work, we explore the use of mild oxidants (CO_2 and H_2O) during the synthesis of graphene over Ni films. The experimental data and theoretical data point to the mild oxidants playing multiple roles. Experimentally, we observe fewer graphene layers than conventional synthesis over Ni. First-principles calculations and XPS data show the formation of a suboxide a little below the Ni surface. This acts as a diffusion barrier for C species. Indeed, the data points to graphene formation being dominated by surface diffusion rather than bulk diffusion. In addition, our calculations demonstrate an increased catalytic activity at the surface suggesting the surface decomposition of the feedstock (CH_4) and graphene formation at the surface should be efficient. This is in keeping with our experimental observations where we are able to obtain graphene at the relatively low temperature of 700 °C. Moreover, we obtain very high quality graphene at this low temperature as indicated by a minute D band peak in the obtained Raman spectra. All these aspects, namely, diminished bulk diffusion, increased catalytic activity enabling reduced synthesis temperatures, and high quality graphene, make the use of mild oxidants in the CVD synthesis of graphene highly attractive. These studies highlight the need for mild oxidants to be further exploited in CVD grown graphene on a broader scale.

EXPERIMENTAL SECTION

The Nickel films were grown over a Si/SiO_2 substrate using electron beam evaporation. The film thickness was 300 nm thick. For synthesis, a vertical fixed-bed quartz tube furnace was used (see Supporting Information Figure S1). The bed in which the substrate resided was made of quartz with holes (*i.e.*, a sieve of approximately 100 mesh). The gas was injected from the top of the reactor. The optimized synthesis protocol is also provided

in Supporting Information Figure S1). Initially, the system is heated (23 °C/min.) in H_2 at a flow of 300 sccm. Once it reaches 700 °C, it remains at this temperature for 30 min. At this point, the gas mixture for the reaction commences and consists of 100 sccm CH_4 with 200 sccm H_2 or 100 sccm CH_4, 100 sccm CO_2 with 100 sccm N_2. This allowed us to compare the role of CO_2. The gas flow rates chosen are optimized for growth without CO_2. After the reaction, the reactor was flooded with N_2, and then after a further 30 min, the system was cooled. Cooling rates from 300 to 40 °C/min were explored. No discernible differences were observed.

Once cooled to room temperature, the as-prepared samples were subjected to a variety of characterizations. Raman spectra were acquired with a Renishaw InVia micro-Raman spectrometer at ambient conditions. A 514 nm wavelength Ar-ion laser was used as the excitation source and the incident power was limited to 2 mW to minimize heating effects and damaging the graphene. The spectral resolution is ~1 cm^{-1}. Peak intensities, peak positions and deconvoluted peaks were extracted with WiRE 3.3 software.

The electronic structure of graphene/Ni interface was investigated by depth profile XPS using a newly developed Argon Gas Cluster Ion Beam GCIB sputtering process to avoid any chemical structure damage. XPS measurements were carried out in the same UHV analysis system (Versaprobe PHI 5000 manufactured by ULVAC-PHI), where the Ar GCIB and Ar ions sputtering guns were placed. Depth profile analysis were performed by a sequenced Ar GCIB (5 keV, 2500 Ar atoms/cluster) and Arions (1 keV) sputtering from the surface to the bulk with a sputtering step of 10 s. The XPS analysis were performed at 45° takeoff angle using a focused (diameter of the irradiated area = 100 μm) monochromatized Al Kα radiation (1486.6 eV). The spectrometer was calibrated using the photoemission lines of gold (Au $4f_{7/2}$ = 83.9 eV, with reference to the Fermi level) and silver (Ag $3d_{5/2}$ = 368.3 eV). For the Au $4f_{7/2}$ lines, the full width at half-maximum (fwhm) was 0.86 eV. The core peaks and valence bands were recorded with constant pass energy of 23 eV. The reader should note that while the XPS depth profiling studies are conducted at UHV conditions, they are not actually obtained during the CVD reaction. Thus, the XPS data may not be representative of the true chemistry of the surface and subsurface occurring during the actual CVD reaction.

The TEM investigations were conducted in a third-order aberration corrected (objective lens) FEI Titan 300−80 operating with an acceleration voltage of 80 kV. Electron energy loss spectroscopy was conducted on a Gatan Tridem 685 ER

Details of the computational studies are as follows:

DFT calculations were utilized to evaluate the CO_2 or CH_4 interaction on the Ni surface with a periodic slab model to describe the interaction between reactant gases and the catalyst so as to determine which gas undergoes a more preferable reaction at the catalyst surface. In addition, we studied the reaction pathway for the CH_4 decomposition and the energy profile of carbon diffusion on Ni and NiO_x. The geometry optimizations were performed using the CASTEP module under the following conditions: (i) the general gradient approximation (GGA) was at the PBE level for functional options with spin polarized calculations, (ii) 340 eV for the basis set was employed to predict the properties of the catalyst and reactants, and (iii) ionic cores were determined by the ultrasoft pseudopotential.

For the quantum calculations, three-dimensional models were employed. After the initial atomic positions were assigned, geometry optimization was carried out to refine the model structure without constraints. The vacuum thickness (size of unit cell perpendicular to slab−slab thickness) was set to 30 Å for all calculations. The convergence SCF tolerance is 1×10^{-6} eV/atom, and special k points of Ni (111) and NiO_x (111) system were chosen as $4 \times 4 \times 1$ and $10 \times 1 \times 10$, respectively. Hubbard U correction to 4.6 eV was applied to improve the description of the electronic structure of Ni-3d orbitals.

The calculated binding energy shows the interaction properties of the reactant with the catalyst. The binding energy, ΔE_b, between the catalyst and reactant surface were determined by three single total energy calculations: (i) geometry optimization of the reactant, (ii) geometry optimization of the catalyst without the reactant, and (iii) geometry optimization of the catalyst with the reactant. The binding energy was determined as follows:

$$\Delta E_b = E_{catalyst+reactant} - (E_{catalyst} + E_{reactant}) \quad (1)$$

where ΔE_b denotes the binding energy of the reactant gas on the catalyst and $E_{catalyst+reactant}$, $E_{catalyst}$, and $E_{reactant}$ are the energy of the reactant adsorbed on the catalyst, the energy of catalyst without reactant, and the energy of the single reactant, respectively.

Conflict of Interest: The authors declare no competing financial interest.

Acknowledgment. This work was supported by the Institute of Basic Science (IBS) Korea. A.B. thanks the Foundation for Polish Science for the financial support within the frames of the Homing Plus Programme (Grant agreement: HOMING PLUS/2013-7/2). M.H.R. acknowledges the Sino-German Center for Research Promotion (Grants GZ 871).

Supporting Information Available: Schematics on the experimental setup and protocol, various addition experimental data (SEM and Raman Spectroscopy) as well as addition theoretical studies. This material is available free of charge *via* the Internet at http://pubs.acs.org.

REFERENCES AND NOTES

1. *ASM Handbook: Alloy Phase Diagrams*; Massalski, T. B., Okamoto, H., Subramanian, P. R., Kacprzak, L., Eds.; ASM International: Materials Park, OH, 2002, Vol. 3.
2. Baraton, L.; He, Z. B.; Lee, C. S.; Cojocaru, C. S.; Châtelet, M.; XMaurice, J. L.; Lee, Y. H.; Pribat, D. On the Mechanisms of Precipitation of Graphene on Nickel Thin Films. *EPL* **2011**, *96*, 46003–46009.
3. Lander, J. J.; Kern, H. E.; Beach, A. L. Solubility and Diffusion Coefficient of Carbon in Nickel: Reaction Rates of Nickel-Carbon Alloys with Barium Oxide. *J. Appl. Phys.* **1952**, *23*, 1305–1309.
4. Zhang, Y.; Zhang, L. Y.; Zhou, C. W. Review of Chemical Vapor Deposition of Graphene and Related Applications. *Acc. Chem. Res.* **2013**, *46*, 2329–2339.
5. Warner, J. H. Schaffel, F.; Rümmeli, M. H.; Bachmatiuk, A. *Graphane: Fundamentals and Emergent Applications*; Elsevier: New York, 2013, ISBN: 978-0-12-394593-8.
6. Rümmeli, M. H.; Zeng, M.; Melkhanova, S.; Gorantla, S.; Bachmatiuk, A.; Fu, L.; Yan, C. L.; Oswald, S.; Mendes, R. G.; Makarov; *et al.* Insights into the Early Growth of Homogeneous Single-Layer Graphene over Ni−Mo Binary Substrates. *Chem. Mater.* **2013**, *25*, 3880–3887.
7. Dai, B.; Fu, L.; Zou, Z.; Wang, M.; Xu, H.; Wang, S.; Lin, Z. Rational Design of a Binary Metal Alloy for Chemical Vapour Deposition Growth of Uniform Single-Layer Graphene. *Nat. Commun.* **2011**, *2*, 522–527.
8. Weatherup, R. S.; Bayer, B. C.; Blume, R.; Ducati, C.; Baehtz, C.; Schlögl, R.; Hofmann, S. *In Situ* Characterization of Alloy Catalysts for Low-Temperature Graphene Growth. *Nano Lett.* **2011**, *11*, 4154.
9. Zhao, P.; Hou, B.; Chen, X.; Kim, S. J.; Chiashi, S. H.; Einarssonab, E.; Maruyama, S. G. Investigation of Non-Segregation Graphene Growth on Ni *via* Isotope-Labeled Alcohol Catalytic Chemical Vapor Deposition. *Nanoscale* **2013**, *5*, 6530–6537.
10. Weatherup, R.; Dlubak, B.; Hofmann, S. Kinetic Control of Catalytic CVD for High-Quality Graphene at Low Temperatures. *ACS Nano* **2012**, *6*, 9996–10003.
11. Baraton, L.; He, Z. B.; Lee, C. S.; Maurice, J. L.; Cojocaru, C. S.; Gourgues-Lorenzon, A. F.; Lee, Y. H.; Pribat, D. Synthesis of Few-Layered Graphene by Ion Implantation of Carbon in Nickel Thin Films. *Nanotechnology* **2011**, *22*, 085601.
12. Hata, K.; Futaba, D. N.; Mizuno, K.; Namai, T.; Yumura, M.; Iijima, S. Water-Assisted Highly Efficient Synthesis of Impurity-Free Single-Walled Carbon Nanotubes. *Science* **2004**, *306*, 1362–1364.

13. Wu, Z. P.; Wang, J. N.; Ma, J. Methanol-Mediated Growth of Carbon Nanotubes. *Carbon* **2009**, *47*, 324–327.
14. Z hang, G. Y.; Mann, D.; Zhang, L.; Javey, A.; Li, Y. M.; Yenilmez, E.; Wang, Q.; McVittie, J. P.; Nishi, Y.; Gibbons, J.; Dai, H. J. Ultra-High-Yield Growth of Vertical Single-Walled Carbon Nanotubes: Hidden Roles of Hydrogen and Oxygen. *Proc. Natl. Acad. Sci. U.S.A.* **2005**, *102*, 16141–16145.
15. Murakami, Y.; Chiashi, S.; Miyauchi, Y.; Hu, M. H.; Ogura, M.; Okubo, T.; Maruyama, S. Growth of Vertically Aligned Single-Walled Carbon Nanotube Films on Quartz Substrates and Their Optical Anisotropy. *Chem. Phys. Lett.* **2004**, *385*, 298–303.
16. Amama, P. B.; Pint, C. L.; McJilton, L.; Kim, S. M.; Stach, E. A.; Murray, P. T.; Hauge, R. H.; Maruyama, B. Role of Water in Super Growth of Single-Walled Carbon Nanotube Carpets. *Nano Lett.* **2009**, *9*, 44–49.
17. Yamada, T.; Maigne, A.; Yudasaka, M.; Mizuno, K.; Futaba, D. N.; Yumura, M.; Iijima, S.; Hata, K. Revealing the Secret of Water-Assisted Carbon Nanotube Synthesis by Microscopic Observation of the Interaction of Water on the Catalysts. *Nano Lett.* **2008**, *8*, 4288–4292.
18. Huang, J.; Zhang, Q.; Zhao, M. Q.; Wei, F. Process Intensified Cation by CO_2 for High Quality Carbon Nanotube Forest Growth: Double-Walled Carbon Nanotube Convexity or Single-Walled Carbon Nanotube Bowls. *Nano Res.* **2009**, *2*, 872–881.
19. Liao, C. D.; Lu, Y. Y.; Tamalampudi, S. R.; Cheng, H. C.; Chen, Y. T. Chemical Vapor Deposition Synthesis and Raman Spectroscopic Characterization of Large-Area Graphene Sheets. *Chem. J. Phys. Chem. A* **2013**, *117*, 9454–9461.
20. Li, X. S.; Cai, W. W.; Colombo, L. G.; Ruoff, R. S. Evolution of Graphene Growth on Ni and Cu by Carbon Isotope Labeling. *Nano Lett.* **2009**, *9*, 4268–4272.
21. Kalbac, M.; Kong, J.; Dresselhaus, M. S. Large Variations of the Raman Signal in the Spectra of Twisted Bilayer Graphene on a BN Substrate. *J. Phys. Chem. C* **2012**, *116*, 19046–19050.
22. Goto, Y.; Taniguchi, K.; Omata, T.; Otsuka-Yao-Matsuo, S.; Ohashi, N.; Ueda, S.; Yoshikawa, H.; Yamashita, Y.; Oohashi, H.; Kobayashi, K. Formation of Ni_3C Nanocrystals by Thermolysis of Nickel Acetylacetonate in Oleylamine: Characterization Using Hard X-ray Photoelectron Spectroscopy. *Chem. Mater.* **2008**, *20*, 4156–4160.
23. Bachmatiuk, A.; Boerrnert, F.; Grobosch, M.; Schaeffel, F.; Wolff, U.; Scott, A.; Zaka, M.; Warner, J. H.; Klingeler, R.; Knupfer, M.; *et al* Investigating the Graphitization Mechanism Of SiO_2 Nanoparticles in Chemical Vapor Deposition. *ACS Nano* **2009**, *3*, 4098–4104.
24. Oswald, S.; Brückner, W. XPS Depth Profile Analysis of Non-Stoichiometric NiO Films. *Surf. Interface Anal.* **2004**, *36*, 17–22.
25. Bystrzejewski, M.; Schönfelder, R.; Cuniberti, G.; Lange, H.; Huczko, A.; Gemming, T.; Pichler, T.; Büchner, B.; Rümmeli, M. Exposing Multiple Roles of H_2O in High-Temperature Enhanced Carbon Nanotube Synthesis. *Chem. Mater.* **2008**, *20*, 6586–6588.
26. Noda, T.; Inagaki, M. Effect of Gas Phase on Graphitization of Carbon. *Carbon* **1964**, *2*, 127–130.
27. Hüfner, S. *Photoelectron Spectroscopy Principles and Application*; Springer-Verlag: Berlin Heidelberg, 1995.
28. Mueller, J. E.; van Duin, A. C. T.; Goddard, W. A. Structures, Energetics, and Reaction Barriers for CH_x Bound to the Nickel (111) Surface. *J. Phys. Chem. C* **2009**, *113*, 20290–20306.
29. Hao, Y.; Bharathi, M. S.; Wang, l.; Liu, Y.; Chen, H.; Nie, S.; Wang, X.; Chou, H.; Tan, C.; Fallahazad, B.; *et al.* The Role of Surface Oxygen in the Growth of Large Single-Crystal Graphene on Copper. *Science* **2013**, *342*, 720–723.